Competition between band gap and yellow luminescence in GaN and its relevance for optoelectronic devices

W. Grieshaber,[a] E. F. Schubert, and I. D. Goepfert
Center for Photonics Research and Department of Electrical and Computer Engineering, Boston University, Boston, Massachusetts 02215

R. F. Karlicek, Jr., M. J. Schurman, and C. Tran
Emcore Corporation, Somerset, New Jersey 08873

(Received 6 May 1996; accepted for publication 8 July 1996)

The competition between band gap and the 2.2 eV (yellow) luminescence of epitaxial GaN is studied for excitation densities ranging from 5×10^{-6} to 50 W/cm^2. The ratio of the peak intensities of the band gap-to-yellow luminescence changes from 4:1 to 3000:1 as the excitation density is increased by 7 orders of magnitude. At room temperature, the band gap luminescence linewidth is $2.3kT$, close to the theoretical minimum of $1.8kT$. A model is developed describing the intensity of the two radiative transitions as a function of the excitation density. This model is based on bimolecular rate equations and takes into account shallow impurities, deep levels, and continuum states. The theoretically predicted dependences of the two different luminescence channels follow power laws with exponents of $\frac{1}{2}$, 1 and $\frac{3}{2}$. Thus the intensity of the yellow luminescence does not saturate at high excitation densities. These dependences are in excellent agreement with experimental results. The relevance of the results for optoelectronic GaN devices is discussed. It is shown that the peak intensity of the yellow luminescence line is negligibly small at typical injection currents of light-emitting diodes and lasers. [S0021-8979(96)01020-1]

INTRODUCTION

The III-V nitride semiconductors GaN, InN, and AIN have gained considerable attention because of the promising material properties such as high thermal stability, chemical inertness, and mechanical resistance, as well as the recent demonstration of high-efficiency light emitting diodes[1] and lasers[2] emitting in the blue and ultraviolet (UV) part of the optical spectrum. For improved device performance and reliability, the concentration of deep levels caused by native defects, deep impurities, interface defects, and other defects needs to be minimized. In conventional III-V semiconductors, deep levels have played an important role in the research and manufacturing of optoelectronic semiconductor devices. Examples of important deep centers include the EL-2 level in GaAs and the *DX* center in $Al_xGa_{1-x}As$ (Schubert[3]). A considerable research effort had been directed towards the identification of these defects and the understanding of the defect physics.[4]

In GaN, optical characterization by photoluminescence has revealed a dominant defect-assisted transition which emits in a broad band centered at 2.2 eV (''yellow luminescence'').[5–10] The yellow luminescence has been reported for epitaxial layers grown by metalorganic vapor-phase epitaxy (MOVPE) and molecular beam epitaxy (MBE). The intensity of the yellow luminescence depends on the growth conditions.[11,12] At the present time, the microscopic origin of the 2.2 eV luminescence has not been identified. The participation of native defects as well as impurities has been proposed.[5] Other experiments support a shallow-to-deep-donor recombination.[7,8]

In this article, we present a detailed 77 and 300 K photoluminescence study on MOVPE grown GaN. The luminescence intensities of the near-band gap (UV) transition and of the 2.2 eV (yellow) transition are monitored. The high radiative efficiency of the GaN samples allows us to vary the excitation density over 7 orders of magnitude. A model describing the relative intensities of the two luminescence lines is developed. This model is based on bimolecular rate equations and takes into account shallow donors, deep states, and conduction and valence band states. Finally, we discuss the relevance of the yellow luminescence for optoelectronic device applications.

EXPERIMENT

Photoluminescence experiments at $T=77$ and 300 K are performed on nominally 2-μm-thick Si-doped ($n=2\times10^{18}$ cm^{-3}) epitaxial GaN films grown in an Emcore MOVPE system on the *c* plane of a sapphire substrate. The GaN was grown at 1050 °C after the growth of a 0.02 μm GaN buffer grown at about 500 °C. A HeCd laser emitting at 325 nm (3.81 eV) with an output power of 16 mW is used as an excitation source. In order to vary the excitation density, neutral density filters and deliberate focusing and defocusing of the laser beam are employed: the GaN samples are either illuminated with the unfocused HeCd laser beam with 1.5 mm beam diameter, or by the laser beam focused down to a spot of 110 μm in diameter to achieve excitation densities up to 50 W/cm^2. For low-temperature measurements, the samples are mounted on the cold finger of a cryostat cooled to liquid nitrogen temperature. The angle of incidence of the laser beam is 50° off the surface normal of the sample. A 37° cone of the luminescence, emerging at 40° off the sample's

[a]Electronic mail: wolfgrie@bu.edu

 0021-8979/96/80(8)/4615/6/$10.00

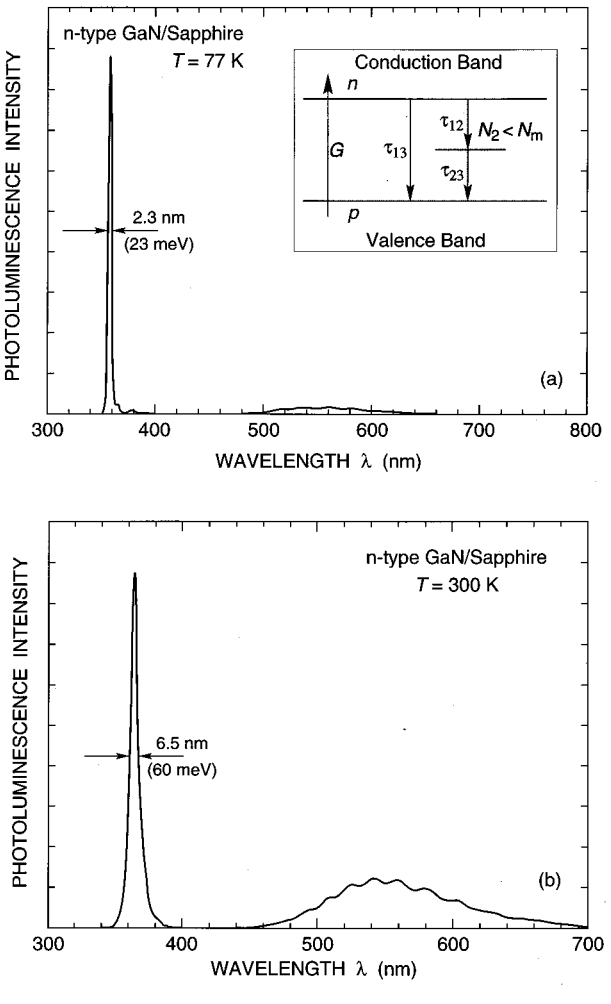

FIG. 1. GaN photoluminescence spectra at 77 K (a) and room temperature (b) under unfocused excitation. The inset shows the 3 levels of the model with their population (n,N_2,p) CB and VB are the conduction and valence band, respectively. Relaxation directions, characteristic time constants (τ_{12}, τ_{23}, τ_{13}), and light induced carrier generation (G) are indicated.

surface normal, is collected and imaged onto the entrance slit of a 0.5 m monochromator. The photoluminescence is detected by a Hamamatsu photomultiplier tube (R-928) followed by a current amplifier.

The intensity of all photoluminescence spectra are carefully recorded allowing a direct comparison of the relative emission intensities for the entire range of excitation intensities covered in this study. At the lowest excitation density, the photoluminescence intensities are accurate to within a factor of 1.5 due to detection and amplification noise.

RESULTS

Figure 1(b) shows a typical GaN room temperature photoluminescence spectrum with an intense near-band gap transition located at 3.405 eV (365 nm) which we hereafter call *UV transition*. Monemar[13] has shown that the temperature dependence of the GaN band gap is given by

$$E_g(T)=3.503\ \text{eV}-\frac{5.08\times10^{-4}(\text{eV/K})T^2}{(996\text{K}-T)}, \qquad (1)$$

which gives $E_g(300\ \text{K})=3.437$ eV. However Gil *et al.*[14] have shown that strain can increase this value by up to 30 meV. The strain is due to the lattice mismatch of the substrate and the GaN epitaxial layer and it depends on the choice of substrate, properties of the buffer layer, growth temperature, and the thickness of the epilayer.

The near-band gap luminescence at room temperature has been interpreted as

(i) a free exciton transition,[9]
(ii) a donor-bound exciton transition,[8,10] or
(iii) a donor-to-valence-band transition.[10]

The full width at half maximum (FWHM) of the UV transition is 60 meV (6.5 nm) which is equal to 2.3 kT at 300 K. This width is close to the theoretical minimum of 1.8 kT valid for thermally broadened band-to-band or impurity-to-band recombination in the absence of stimulated emission and self-absorption processes. The measurement geometry and excitation powers employed here make stimulated emission and self-absorption processes negligible.

Figure 1 also reveals a second luminescence line centered around 2.2 eV (560 nm). We attribute the oscillating structure on the yellow luminescence band to intensity modulation by the Fabry–Perot cavity formed by the air-GaN and GaN-sapphire interface.

The luminescence spectrum at $T=77$ K is shown in Fig. 1(a). The FWHM of the UV transition is reduced to 23 meV which is a remarkably low value. The energy of the UV peak shifts to 3.462 eV (358 nm) at 77 K in agreement with the shift of the energy gap calculated from Eq. (1).

The broadening of the UV peak from 23 meV (77 K) to 60 meV (300 K) is consistent with the three types of transitions mentioned above. However, since the UV transition at 300 K occurs 40 meV below the unstrained band gap, it is unlikely that the UV transition is a free carrier band-to-band transition. Photoreflectance studies are being conducted to identify the nature of the UV transition.

No change in the UV and yellow linewidth results as the excitation density is varied, as inferred from Fig. 2. This allows us to compare the integrated intensities by computing the ratio of the peak intensities. For focused and unfocused excitation, the excitation densities are varied with neutral density filters over a large range to ensure that the excitation density overlaps for the two sets of data (focused and unfocused excitation). In order to display the two sets of data on a single excitation density axis, it is assumed, that the peak ratio depends only on the excitation density and not on the change of excitation area. This assumption is justified because the optical properties of the samples are uniform on the length scale of the unfocused beam diameter, i.e., 1.5 mm.

Figures 3(a) and 3(b) show the UV and ''yellow'' peak intensities normalized to the intensity of yellow photoluminescence at the lowest excitation for each temperature. At $T=77$ K, the UV intensity is approximately 7 times higher than the UV luminescence at $T=300$ K, indicating that nonradiative processes play a role at room temperature. Inspection of Fig. 3(a) reveals a *linear dependence* of the UV *and* the yellow luminescence signal at low excitation densities

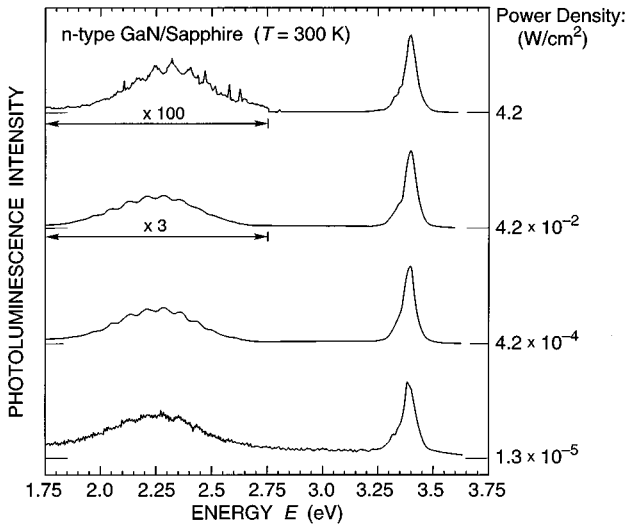

FIG. 2. Room temperature photoluminescence spectra at different excitation densities as indicated on the right-hand ordinate. The intensity of the yellow luminescence (1.75–2.75 eV) is amplified by the factor indicated beneath the band. The line at energies higher than 3.6 eV gives the null intensity of the luminescence.

(straight lines). At excitation densities higher than 10^{-2} W/cm^2, the yellow luminescence turns to a *square-root-dependence* (dashed line), whereas the UV luminescence continues to follow the linear dependence. Figure 4 shows the ratio of UV-to-yellow luminescence. Inspection of Fig. 4 reveals a constant luminescence ratio for low excitation intensities and a square-root dependence at higher intensities. The ratio is consistent with the excitation density dependences outlined above.

MODEL

We next calculate the recombination rates of the two competing recombination channels in GaN by a theoretical model that takes into account

(i) conduction and valence band states,
(ii) deep states involved in the yellow luminescence, and
(iii) shallow donor states.

The inset in Fig. 1(a) shows the band diagram consisting of the conduction and valence band and the deep states. The shallow donor states are assumed to have merged with the continuum of the conduction band. The UV luminescence originates from a near-band gap transition (n being the concentration of electrons in the conduction band, p the concentration of holes in the valence band) and yellow luminescence involves deep states located within the band gap of GaN. We denote N_m as the total concentration of the deep states and N_2 as the concentration of deep states occupied by electrons. The transition *probability* per unit time for one electron to recombine with one hole is τ^{-1} and the transition *rate* increases with the number of occupied initial states and free final states. Thus the following rate equations describe the transitions as *bimolecular* recombinations. The model overcomes the inapplicability of the monomolecular recombination model in the high excitation density regime where

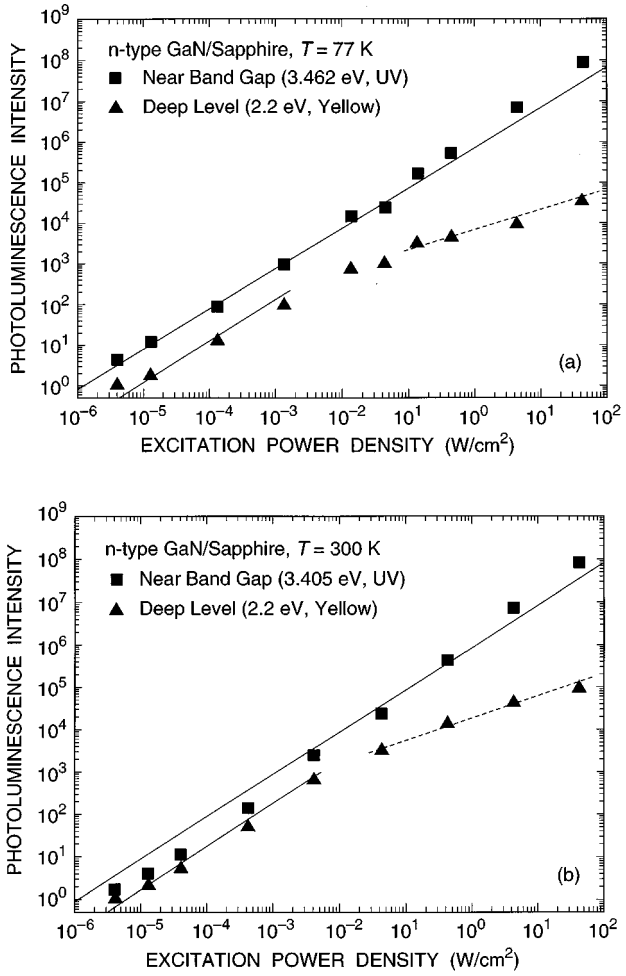

FIG. 3. Measured photoluminescence peak intensities of the UV (squares) and yellow (triangles) luminescence as a function of excitation density at (a) 77 K and (b) room temperature. The intensities have been normalized to the yellow luminescence at lowest excitation density. The lines show the linear dependence (straight line) and square-root dependence (dotted line).

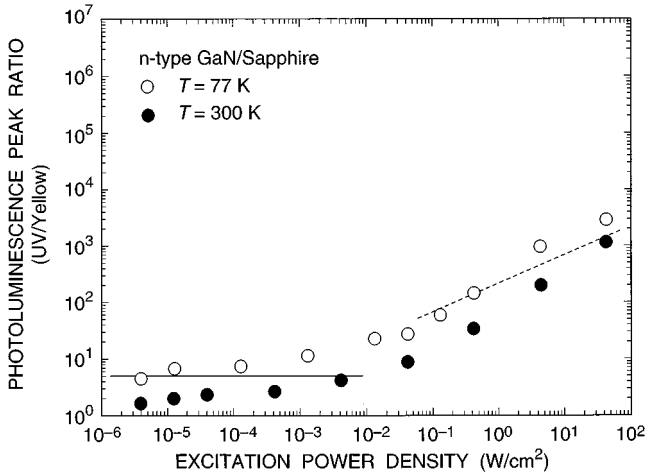

FIG. 4. Ratio of experimental peak intensities as a function of the excitation density in the two excitation regimes, focused (excitation density $>10^{-1}$ W/cm^2), and unfocused (excitation density $<10^{-1}$ W/cm^2), at 77 K and room temperature. The lines show absence of dependence (straight line) and square-root dependence (dotted line).

the free carrier concentrations (n and p) are higher than the doping concentration (N_D). With G being the generation rate of the photoinduced electron-hole pairs, the generation-recombination balance in the steady state is given by:

$$\frac{dn}{dt} = G - V\left(\frac{np}{\tau_{13}} - \frac{n(N_m - N_2)}{\tau_{12}}\right) = 0, \tag{2}$$

$$\frac{dN_2}{dt} = V\left(\frac{n(N_m - N_2)}{\tau_{12}} - \frac{N_2 p}{\tau_{23}}\right) = 0, \tag{3}$$

where Eq. (2) applies to the conduction band and Eq. (3) applies to the deep state. V is a proportionality constant with the dimension of a volume. The magnitude of the constant V is discussed in the Appendix. The rate equation for the hole concentration is given by $dp/dt = -dn/dt - dN_2/dt$ and thus provides no additional information.

Assuming the shallow donor concentration of N_D, the neutrality condition is given by

$$n + N_2 = p + N_D, \tag{4}$$

where we assumed that occupied deep states have the charge state $z = -1$ and all shallow donors are ionized. In the case of compensated semiconductors, N_D in Eq. (4) must be replaced by $N_D - N_A$.

The intensity of the luminescence transitions is proportional to the transition rates:

$$I_{\mathrm{UV}} \propto \frac{np}{\tau_{13}}, \tag{5}$$

$$I_y \propto \frac{N_2 p}{\tau_{23}}. \tag{6}$$

The system of Eqs. (2)–(4) has three positive unknowns (n, p, N_2) and three parameters (G, N_m, N_D). Simple algebraic transformations yield

$$G(N_2) = V\frac{N_2(N_D - N_2)(N_m - N_2)[(N_D - N_2)\tau_{12}\tau_{23} + A\tau_{13}]}{A^2\tau_{13}}, \tag{7}$$

$$n(N_2) = \frac{(N_D - N_2)N_2\tau_{12}}{A}, \tag{8}$$

$$p(N_2) = \frac{(N_D - N_2)(N_m - N_2)\tau_{23}}{A}, \tag{9}$$

where $A = N_2\tau_{12} - (N_m - N_2)\tau_{23}$. For a given doping concentration N_D and total concentration of deep states N_m, N_2 can be systematically varied. The quantities G, n, and p are then calculated from Eqs. (7)–(9). Using this method, the intensity of the two recombination channels, I_{UV} and I_y, is calculated from Eqs. (5) and (6) for a known generation rate G.

Figures 5(a) and 5(b) show the calculated photoluminescence intensities and their ratio as a function of excitation density for a highly n-doped semiconductor and for an intrinsic semiconductor, respectively. In these figures we used $N_m = 10^{15}$ cm^{-3} and $\tau_{13} = \tau_{12} = \tau_{23} = 1$ ns. In Figs. 5(a) and 5(b) the doping concentration N_D is 10^{18} cm^{-3} and 0, respectively. Since the absolute quantum efficiency of the radiative recombination and their temperature dependence are unknown, the calculated PL intensities in Fig. 5 are shifted along the photoluminescence intensity axis to yield the same appearance as the experimental dependences.

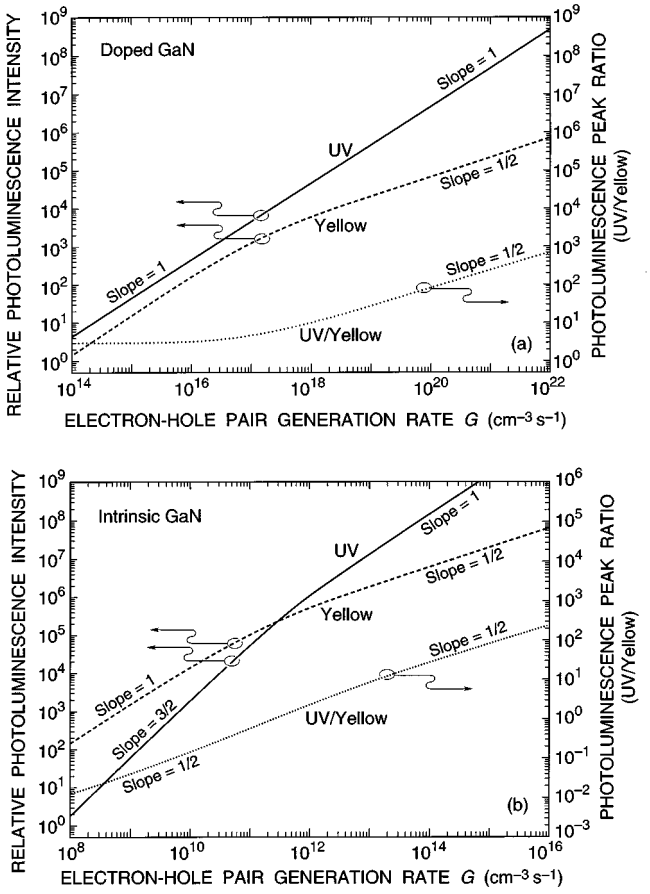

FIG. 5. Calculated luminescence intensities of the near-band gap and the deep level (yellow) luminescence for (a) doped ($N_D = 10^{18}$ cm^{-3}) and (b) intrinsic ($N_D = 0$) semiconductors using Eqs. (5)–(9) with $\tau_{12} = \tau_{23} = \tau_{13} = 1$ ns and $N_m = 10^{15}$ cm^{-3}. The UV and yellow photoluminescence intensity (left ordinate) is shown in continuous and dashed line, respectively, and the luminescence ratio UV/yellow is shown in dotted line on the right ordinate.

The results shown exhibit power law dependences of the luminescence intensities on the carrier generation rate $I \propto G^i$, where i can assume the values $\frac{1}{2}$, 1, or $\frac{3}{2}$. Table I gives the calculated values of i for doped and intrinsic semiconductors in the low and high excitation regime. In the two extreme cases of high and low excitation densities, simplifying assumptions can be made to obtain the exponents of the UV and yellow photoluminescence. One obtains:

(i) *High excitation:* All free carrier concentrations are large and the last term in Eq. (2) can be neglected, yielding both n and p proportional to $\sqrt{G}$. Thus the UV luminescence increases linearly with the excitation density. Then,

TABLE I. Exponents of power-law dependence of luminescence intensities on excitation for different excitation densities and doping concentrations.

Excitation density	Low		High	
Doping	Intrinsic	Highly doped	Intrinsic	Highly doped
band-to-band	3/2	1	1	1
deep-level assisted	1	1	1/2	1/2

in Eq. (3) the $\sqrt{G}$ dependence of n and p cancel out, yielding the high excitation population of level 2: $N_2^{\text{high excit.}}=N_m\tau_{23}/(\tau_{12}+\tau_{23})$. Thus, the population of level 2 saturates, but I_y *does not* since the number of holes p still increases with $\sqrt{G}$. It is worth noting that in the n-type doped case N_2 approaches $N_2^{\text{high excit.}}$ from higher values, and from lower values in the p type or intrinsic case.

(ii) *Low excitation:* In the low excitation regime we have to distinguish between the doped and undoped case.

Doped semiconductor: We assume n-type doping, the level 2 to be completely filled ($N_2\approx N_m$), $n\approx N_D-N_m>0$ and thus p is small. Again the last term in Eq. (2) can be neglected yielding p and both photoluminescence intensities proportional to G. A slightly different argument holds for p doping ($N_D<0$) but leads to the same result.

Intrinsic semiconductor: All populations are small (especially $N_2\ll N_m$), and the np product in Eq. (2) can be neglected leaving $n\propto G$. Inserting this result in Eq. (3) yields $N_2\propto\sqrt{G}$ and $p\propto\sqrt{G}$ and finally $I_{\text{UV}}\propto G^{3/2}$ and $I_y\propto G$. The model described above is restricted to excitation densities at which stimulated emission does not occur.

It is worth noting that if the yellow luminescence involves a transition between two deep levels, the saturation must occur at a sufficiently high excitation density. The lack of yellow luminescence intensity saturation supports our model which assumes only one deep level.

DISCUSSION

The dependences of the UV and the yellow luminescence transitions are shown in Figs. 3(a) and 3(b). Also included in these figures are straight and dashed lines with the slopes 1 (linear dependence) and $\frac{1}{2}$ (square-root dependence), respectively. The power-law for slope 1 provides a good fit for the UV luminescence over the entire range of excitation densities. The yellow luminescence follows a linear dependence for low excitation densities and changes to a square-root dependence at high excitation densities. At high excitation densities, the yellow luminescence intensity increases sublinearly and does not saturate.

The power-law dependences of the two luminescence channels predicted by the model for the doped and the undoped case are summarized in Table I. Comparison of the experimental results shown in Figs. 3(a) and 3(b) with the theoretical results shown in Figs. 5(a) and 5(b) reveals quantitative agreement of the dependences. The experimental slopes of $\frac{1}{2}$ and 1 are in agreement with the slopes predicted by our model for doped semiconductors.

We next discuss the relevance of the yellow luminescence for optoelectronic semiconductor devices. In optoelectronic devices, typical power densities exceed 100 W/cm^2 which correspond to current densities of 30 A/cm^2 for a device voltage of 3.5 V. However, the efficient operation of light-emitting diodes (LEDs) can require much higher current densities in the 1–10 kA/cm^2 range.[15] Semiconductor lasers have threshold current densities of similar magnitude.[2] Using the functional dependences derived in this publication and extrapolating the trend to the power densities outlined above reveals that the ratio of band-to-band luminescence to yellow luminescence will be very large, certainly $\gg$10,000:1.

TABLE II. Comparison of typical current used in light-emitting diodes and lasers with densities used in photoluminescence measurements.

	Typical current density (A/cm^2)
optical excitation	10^1
LED	10^1–5×10^2
Laser threshold	10^3–10^4

The electron-hole generation rate at the highest excitation density (50 W/cm^2) used in this study corresponds to a current density of 13 A/cm^2, assuming that all photons are absorbed in the semiconductor and each photon creates an electron-hole pair. At this excitation density, yellow luminescence is already very weak. A further increase in excitation density would, according to our theoretical model, increase the yellow luminescence band *sublinearly*, i.e., would make it even less significant. At magnitudes of the current densities relevant to optoelectronic devices (see Table II), the intensity of the yellow luminescence band is therefore extremely small.

Our data also show that if the peak ratio UV-to-yellow luminescence is used as a characteristic measure for the quality of epitaxial GaN, care must be taken that comparisons between samples maintain identical excitation conditions.

CONCLUSIONS

The near-band gap and the 2.2 eV (yellow) optical transitions in GaN grown by MOVPE have been studied by photoluminescence experiments. The luminescence peak ratio of near band gap-to-yellow luminescence changes from 4:1 to 3000:1 as the excitation density is increased by 7 orders of magnitude from 5×10^{-6} to 50 W/cm^2. At room temperature, the band gap luminescence has a linewidth of 60 meV corresponding to 2.3 kT, close to the theoretical minimum of 1.8 kT. At 77 K, the band gap luminescence has a linewidth of 23 meV. The energy and the broadening of the near-band gap luminescence is consistent with excitonic and donor-to-band recombination. A theoretical model is developed describing the intensity of the two radiative transitions as a function of the excitation density. This model is based on bimolecular rate equations and is thus not limited to the low excitation case. The model takes into account shallow impurities, deep levels, and continuum states. The theoretically predicted dependences of the two different luminescence channels follow power laws with exponents of $\frac{1}{2}$, 1, and $\frac{3}{2}$ depending on excitation density and doping. These dependences are in excellent agreement with experimental results. The intensity of the yellow luminescence does not saturate at high excitation densities. The relevance of the results for optoelectronic GaN devices is discussed. It is shown that the peak intensity of the yellow luminescence line is negligibly small at typical injection currents of LEDs and lasers.

ACKNOWLEDGMENTS

This work was partially supported by the Office of Naval Research. The authors thank T. D. Moustakas for useful discussions. W.G. acknowledges partial support by the Deutsche Forschungsgemeinschaft (DFG).

APPENDIX

The bimolecular recombination rate[16,17] is given by the product of the concentrations of filled initial states and free final states and a proportionality constant B. The constant B is known as the *bimolecular recombination coefficient*. This coefficient is equivalent to the product of the volume V and the probabilities $1/\tau$ in Eqs. (2) and (3) of this publication. We calculate the magnitude of B by using the van Roosbroeck–Shockley model:[18] $B=R/n_i^2$, where n_i is the intrinsic carrier concentration of the semiconductor and R is the total radiative recombination rate (per cm^3 per s) at thermal equilibrium. We assume that the absorption near the allowed, direct gap of GaN is of the form $\alpha(E)=\alpha_0[(E-E_G)/E_G]^{1/2}$. This expression is used to simplify the Van Roosbroek–Shockley formula. One obtains:

$$R=8\pi c n_{\mathrm{opt}}^3 \alpha_0 \sqrt{\frac{k_B T}{E_G}} \left(\frac{k_B T}{ch}\right)^3 \int_{u_G}^{\infty} \frac{u^2\sqrt{u-u_G}}{e^u}\, du, \qquad (10)$$

where $u=E/k_BT$ and $u_G=E_G/k_BT \gg 1$. Due to the sharp increase of the denominator, only a small energy region close to the band gap contributes to the integral. To estimate the room temperature bimolecular recombination coefficient of GaN, B_{GaN}, we use $n_{\mathrm{opt}}=2.6$, $\alpha_0 \approx 10^5\ \mathrm{cm}^{-1}$ (Dingle *et al.*),[19] and $E_G=3.4$ eV to calculate R. The intrinsic carrier concentration n_i is calculated in the parabolic band approximation and we use the effective masses[20] $m_e^*=0.2m_0$ and $m_n^*=0.6m_0$ yielding $B_{\mathrm{GaN}}=7\times10^{-10}\ \mathrm{cm}^3/\mathrm{s}$. With our estimated probability per unit time of $\tau^{-1}=10^9\ \mathrm{s}^{-1}$ we obtain $V=7\times10^{-19}\ \mathrm{cm}^3$. This value is used for the calculations shown in Fig. 5. Due to the approximation made for $\alpha(E)$ and due to the uncertainty on the exact material constants, we estimate B_{GaN} to be accurate within one order of magnitude. Performing the same calculation for GaAs yields $B_{\mathrm{GaAs}}=10^{-9}\ \mathrm{cm}^3/\mathrm{s}$ in reasonable agreement with experiment and exact calculations where $B_{\mathrm{GaAs}}=2\times10^{-10}\ \mathrm{cm}^3/\mathrm{s}$ was obtained.[17,18]

[1] S. Nakamura, M. Senoh, N. Iwasa, and S. Nagahama, Appl. Phys. Lett. **67**, 1868 (1995).
[2] S. Nakamura, M. Senoh, S. Nagahama, N. Iwasa, T. Yamada, T. Matsushita, H. Kiyoku, and Y. Sugimoto, Jpn. J. Appl. Phys. **35**, L74 (1996).
[3] E. F. Schubert, *Doping in III-V Semiconductors* (Cambridge University Press, Cambridge, 1993).
[4] S. T. Pantalides, *Deep Centers in Semiconductors* (Gordon and Breach, Philadelphia, PA, 1992).
[5] R. Singh, R. J. Molnar, M. S. Ünlü, and T. D. Moustakas, Appl. Phys. Lett. **64**, 336 (1994).
[6] X. Zhang, P. Kung, and M. Razeghi, Mat. Res. Soc. Symp. Proc. **395**, 625 (1995).
[7] T. Suski, P. Perlin, H. Tesseyre, M. Leszczynski, I. Grzegory, J. Jun, M. Bockowski, S. Porowski, and T. Moustakas, Appl. Phys. Lett. **67**, 2188 (1995).
[8] D. M. Hofmann, D. Kovalev, G. Steude, B. K. Meyer, A. Hoffmann, L. Eckey, R. Heintz, T. Detchprom, H. Amano, and I. Akasaki, Phys. Rev. B **52**, 16702 (1995).
[9] S. Chichibu, T. Azuhata, T. Sota, and S. Nakamura, J. Appl. Phys. **79**, 2784 (1996).
[10] G. D. Chen, M. Smith, J. Y. Lin, H. X. Jiang, A. Salvador, B. N. Sverdlov, A. Botchkarv, and H. Morkoç, J. Appl. Phys. **79**, 2675 (1996).
[11] A. Botchkarev, A. Salvador, B. Sverdlov, J. Myoung, and H. Morkoç, J. Appl. Phys. **77**, 4455 (1995).
[12] X. Zhang, P. Kung, and M. Razeghi (to be published in Mat. Res. Soc. Symp. Proc. Boston, Fall 1995).
[13] B. Monemar, Phys. Rev. B **10**, 676 (1974); see also O. Madelung in *Data in Science and Technology*, edited by R. Poerschke (Springer, Berlin, 1993), p. 87.
[14] B. Gil, O. Briot, and R.-L. Aulombard, Phys. Rev. B **52**, 17028 (1995).
[15] R. H. Saul, T. P. Lee, and C. A. Burrus, in *Semiconductors and Semimetals*, edited by R. K. Willardson and A. C. Ber (Academic, Orlando, 1985), Vol. 22, part C.
[16] L. A. Coldren and S. W. Corzine, *Diode Lasers and Photonic Integrated Circuits* (Wiley, New York, 1995).
[17] N. K. Dutta, in *Semiconductors and Semimetals* (Academic, San Diego, 1993), Vol. 39.
[18] W. van Roosbroeck and W. Shockley, Phys. Rev. **94**, 1558 (1954).
[19] R. Dingle, D. D. Sell, S. E. Stokowski, P. J. Dean, and R. B. Zetterstrom, Phys. Rev. B. **3**, 497 (1971).
[20] S. Sze, *Physics of Semiconductor Devices*, 2nd ed. (Wiley, New York, 1981).